University of Zurich[UZH]

Integration of satellite based sun-induced chlorophyll fluorescence measurements to improve global transpiration modeling

GEO 610 Master's Thesis

Author
Luc Jerome Sierro
15-931-744

Supervised by
Prof. Dr. Alexander Damm

Faculty representative
Prof. Dr. Alexander Damm

31.12.2022
Department of Geography, University of Zurich

Abstract

Evapotranspiration (ET) is a major component in global cycles such as the carbon, energy and hydrological cycle. Accurately estimating the spatiotemporal behavior of ET is of ever-increasing relevance for water resource management and especially in matters of plant use efficiency. While point measurements of ET allow for a high temporal resolution, they are spatially restricted. Spaceborne remote sensing techniques offer to perform cost-effective data acquisition in both spatial and temporal resolution. Current approaches of using satellite-based information, however, only allow for an estimation of potential rather than actual ET. Hence, attempts are being made to move away from models based on indices such as plant greenness to instead exploiting direct biophysiological processes. Sun-induced fluorescence (SIF) is a variable, which is measurable from space, and has been proposed to be a promising variable to bridge this gap from potential to actual ET. In this thesis, we examine the applicability of SIF for filling this gap by building and comparing several models to incorporate SIF into the Penman-Monteith (PM) based FAO reference crop ET model. We therefore calculated multiple linear regression models between SIF and corresponding parameters from the PM equation. Using best-fit linear regression parameters, we re-scaled the SIF values to the range of the replaced parameter in the equation. While our models were able to represent a reasonable seasonal cycle, they were not able to improve ET estimates on a reliable level. This might be due to the models being based on linear regression, which we assume to not accurately reproduce the complex relationships between meteorological and plant physiological parameters. Future studies should therefore focus on finding better-suited regression models. Also, we recommend future research to incorporate land-cover information in the model to allow adjustments for plant-specific parameters.

Contents

List of Figures

List of Tables

Nomenclature and Abbreviations

CORINE	Coordination of Information on the Environment
C_p	Specific heat of air
Δ	Slope of vapor pressure curve
ε	Ratio of molecular weight of water vapor/dry air
EC	Eddy Covariance
ECMWF	European Centre for Medium-Range Weather Forecasts
ERA5	Fifth generation ECMWF Re-Analysis
e_a	Actual vapor pressure
e_s	Vapor pressure of saturated air
ET	Evapotranspiration
FAO	Food and Agriculture Organization of the United Nations
G	Ground heat flux
γ	Psychrometric constant
JPL	Jet Propulsion Laboratory
λ	Latent heat of vaporization
$LAI_{(active)}$	(Active) Leaf Area Index
LGS	Length of Growing Season
NASA	National Aeronautics and Space Administration
P	Atmospheric Pressure
PM	Penman-Monteith
PT	Priestley-Taylor
R^2	Coefficient of determination
r_a	Aerodynamic resistance
RH	Relative Humidity
RMSE	Root Mean Squared Error
R_n	Net radiation at the surface
r_s	Surface resistance
SIF	Sun-Induced chlorophyll Fluorescence
T	Temperature
T_d	Dew-point temperature
TROPOMI	TROPOspheric Monitoring Instrument
u_2	Wind speed at 2m height
VPD	Vapor Pressure Deficit

1. Introduction

Evapotranspiration (ET) is the process by which water is transferred from the Earth's surface to the atmosphere through evaporation of water from the surface and the transpiration of water from plants. Transpiration accounts for about 61% (± 15% standard deviation) in terrestrial ET (Schlesinger and Jasechko, 2014). Evapotranspiration is not only an important factor in the global carbon and energy cycle (Sellers *et al.*, 1997), but furthermore, plays a crucial role in the global water cycle and is a key factor in determining the amount of water available for agricultural, industrial, and domestic use. Accurate estimation of ET is crucial to a more detailed understanding of plant water use efficiency and carbon cycling (Fisher *et al.*, 2017; Shan *et al.*, 2021).

On a local scale, it is possible to make precise ET measurements using eddy covariance (EC) towers, which consist of several different sensors that measure, for example, flows of gas, solar radiation or also temperature and precipitation, as well as wind speeds (Pastorello *et al.*, 2020). While these EC systems provide us with continuous, high-resolution data over time, these values are only representative of a relatively small footprint (400m – 1km depending e.g., on wind speed and direction) and may not accurately represent a whole ecosystem being studied, which is typically not homogenous (Barcza *et al.*, 2009). However, if we are interested in large-scale measurements, it becomes difficult to extrapolate measurements from a single EC tower or to interpolate measurements from multiple towers. To avoid this problem, it is worthwhile to resort to satellite-based measurements. Remote sensing is considered a powerful tool for estimating ET, as it generally allows for the measurement of large areas over time using spaceborne imagery (Lillesand, Kiefer and Chipman, 2015). By combining satellite imagery with meteorological data and land cover data, it is possible to model ET on the surface (Anderson *et al.*, 2011; Leng *et al.*, 2017). Such models are important because they provide a means to accurately estimate ET over large areas and can be used to monitor and predict changes in ET over time. In recent years, there has been an increasing demand for accurate and reliable ET models to support water resource management and decision-making on a political scale (Hassanzadeh *et al.*, 2014). This is especially true in arid and semi-arid regions, where water is a scarce resource and accurate ET estimation is critical for managing water resources and mitigating the impacts of drought (Yassen, Nam and Hong, 2020). However, despite the importance of such ET models, there are still many challenges and limitations to their development and use, including the complexity of the ET process, the need for accurate and reliable input data, and the need of robust validation and testing of the models (Amatya *et al.*, 2016).

Two of the commonly used calculation methods to estimate ET on a global scale include variations of the Priestley-Taylor (PT) (Priestley and Taylor, 1972) and the Penman-Monteith (PM) (Penman, 1948; Monteith, 1965) approach. While the PM-method takes into account the combined effects of radiation, humidity, temperature and wind on the energy balance at the surface, the PT-method is a simpler method estimating ET based on the net radiation and the difference between the atmospheric and soil vapor pressure. While the PT-approach is easier to implement, requiring fewer input data,

the PM-approach is generally considered to be the more accurate method for calculating ET (Ngongondo *et al.*, 2013). Therefore, the PM-method is recommended for use in circumstances, where data availability and computational resources are given (Utset *et al.*, 2004). To calculate ET in a globally applicable method, the Food and Agriculture Organization (FAO) of the United Nations provides a standardized model to calculate reference ET using the PM-equation, which is internationally recognized as the standard method (Allen *et al.*, 2006; Tanny, 2022). This complex equation consists of many input parameters, such as the net radiation at the crop surface, soil heat flux, daily air temperature at 2m height, saturation vapor pressure, actual vapor pressure, saturation vapor pressure deficit, slope of vapor pressure curve and the psychrometric constant, most of which are still associated with large uncertainties (Allen *et al.*, 1998; Zotarelli *et al.*, 2010; Talebmorad *et al.*, 2020).

While current state-of-the art models can only estimate the potential ET using different vegetation indices, intensive research has been done in recent years on how to get closer to an estimate of the actual ET (Damm, Roethlin and Fritsche, 2018). Potential evapotranspiration is a measure of the amount of water that could be lost from an environment through evaporation and transpiration (water loss through plants) in a given area over a certain period of time, under specific weather conditions. It is a theoretical value that represents the maximum amount of water that could be lost from a given area, if there were no limiting factors, such as drought or water availability. Actual evapotranspiration, however, is the amount of water that is actually lost through evaporation and transpiration in a given area over a certain period of time. It is the measurable amount of water that is lost though ET, thereby taking into account all the limiting factors that affect water availability, such as drought, water availability, and other environmental conditions (Potential Evapotranspiration | Did You Know? | National Centers for Environmental Information (NCEI), 2022).

Studies had been conducted, trying to measure the PM parameters more accurately and with higher spatiotemporal resolution using remote sensing (Zhang, Kimball and Running, 2016). Research has also been conducted to further improve estimates of parameters, that cannot be measured directly using remote sensing approaches, such as e.g. stomatal resistance (r_s) (Niyogi *et al.*, 1997). As r_s is a biological factor (Lei *et al.*, 2018) that responds to any factor influencing the leaf water potential, such as changes in humidity, soil moisture and plant water transport, this parameter of the PM-equation is especially difficult to assess and uncertainties are introduced to the estimation of ET (Buckley, 2019). While the FAO standard model for reference ET suggests a specific value for r_s from a single leaf of 100ms^{-1} under well-watered conditions, and a value of 70 ms^{-1} for the (bulk) surface resistance (Allen *et al.*, 1998), Shan *et al.* (2021) have tried to estimate r_s using a novel proxy for photosynthetic activity, which is sun-induced fluorescence (SIF). While the FAO reference approach is only able to calculate potential ET rather than actual ET, the use of SIF in the estimation of ET

promises to move us nearer to estimates of actual ET (Lu *et al.*, 2018; Zhou *et al.*, 2022). However, the complexity of the process and the many factors that all interact makes implementing SIF in ET estimation particularly difficult (Damm *et al.*, 2018). While SIF may contribute to an improved understanding of the ET process, too little is known about the complex processes within vegetation and assumptions still need to be made (Jarvis and Davies, 1998; Li *et al.*, 2020).

In this thesis, we will explore the importance of ET models in remote sensing, the challenges and limitations of developing and using these models, and the potential avenues for improving their accuracy and reliability. We will investigate the feasibility of using satellite-based SIF measurements to improve global transpiration modeling and assess challenges and limitations of current approaches to estimate ET. We will develop and test new methods for integrating satellite-based SIF measurements into an ET model and evaluate the potential benefits of these methods. The results of this research will provide valuable insights into the potential of SIF measurements for improving global transpiration modeling. This work has the potential to enhance our understanding of the hydrological cycle and to improve the accuracy of climate predictions.

2. Data and Methods

2.1 Data

2.1.1 Study Site

The study area extends from 30° N to 75° N, and -15° E to 45° E (WGS 84) and encompasses the continent of Europe, as well as the northernmost part of Africa. The research site covers land cover classes ranging from artificial surfaces, over agricultural areas, forests and wetlands to the Sahara Desert (Eurostat, 2021). The ecological zones of the study site range from polar, boreal, to temperate and subtropical (Bohn, Hettwer and Gollub, 2005). This highly diverse and dynamic environment makes the study site highly suitable for testing ET models. Several specific locations in different biomes were selected to allow a more precise time-series analysis of the different models over various land cover classes and at different latitudes.

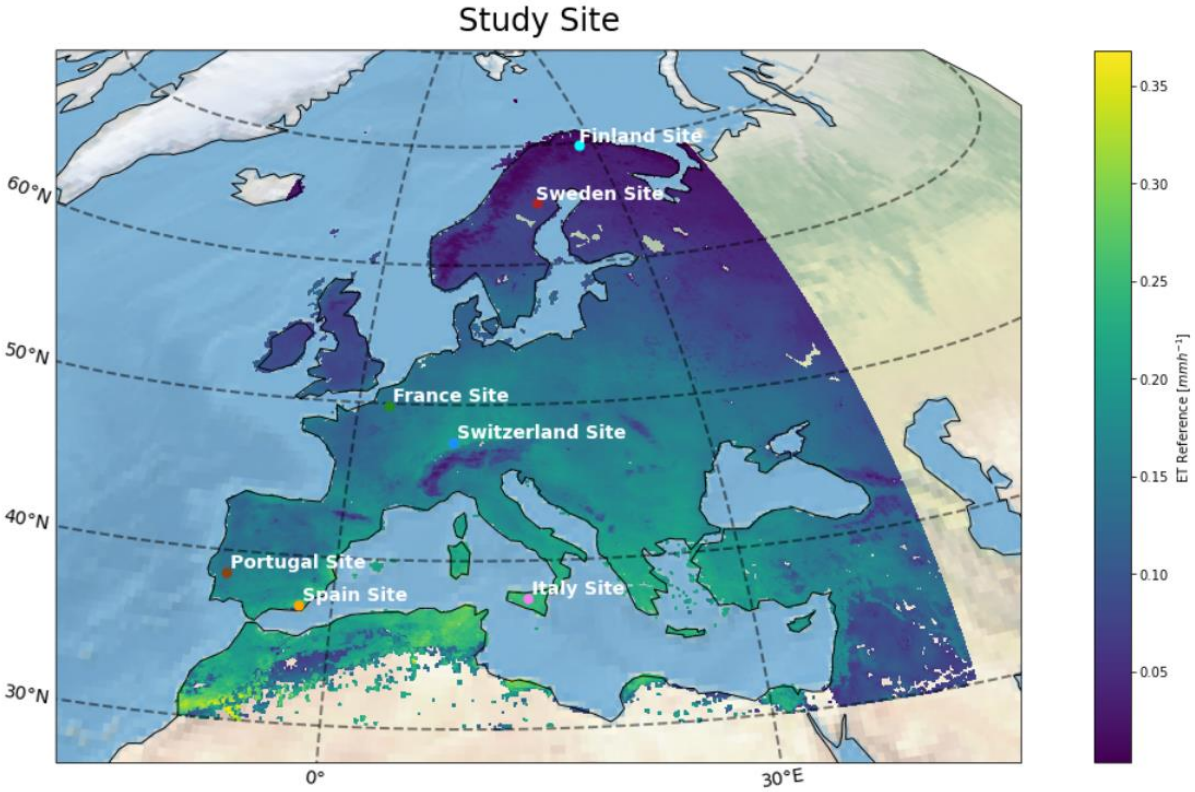

*Figure 1 ET-map for the 01.04.2018 calculated using the FAO crop reference ET model (see chapter 2.2.2), showing marked locations for more detailed timeseries analysis; base map created using the Python SciTools's Cartopy 0.18.0 (*Elson et al., *2020)*

Table 1 Specific sites and their coordinates for in-depth analysis (from north to south)

Location	Latitude	Longitude
Finland Site	69.800	27.640
Sweden Site	64.605	18.362
France Site	49.838	2.639
Switzerland Site	47.478	8.364
Portugal Site	38.610	-8.116
Italy Site	37.697	13.984
Spain Site	37.000	-2.439

In order to better understand the validity of the generated ET time series and to accurately identify correspondingly typical vegetation cycles, a more detailed description of the selected sites is provided here. The here presented land cover information was retrieved from the European Commission's Coordination of Information on the Environment (CORINE) Land Cover inventory CLC2018 (Büttner *et al.*, 2017).

The sites differ not only in longitude and latitude, but also substantially in land surface cover. The Finland site is located in the Kaldoaiavi Wilderness Area, the largest wilderness area in Finland, covered mainly by grasslands and small shrubs. Further south in Swedish Lapland, we find clustered boreal coniferous forest among larger grassland areas. Both Nordic sites contain streams, rivers and smaller lakes. The French site is located west of Amiens in the midst of an agricultural landscape of northern France. The Swiss site is located on the Laegern hill ridge northwest of Zurich, which is covered by a managed mixed deciduous forest and occasional spruce and fir trees. The site in Portugal, located east of Lisbon, includes hardwood forest as well as mixed species forests and agricultural land (Bento-Gonçalves *et al.*, 2018). The Italian site is located in the center of the island of Sicily in the metropolitan region of Palermo and is characterized by intensive agriculture. The southernmost site is located in Spain in the Tabernas Desert, which is covered in parts by shrub- and grassland.

2.1.2 Working Environment

All processing and computing of the necessary data was done in the form of a Python code in the Jupyter Notebook Environment (Kluyver *et al.*, 2016). The code is mainly based on the Xarray package (Hoyer and Hamman, 2017) and Matplotlib v3.4.3 (Caswell *et al.*, 2021). Scikit-learn 1.0.2 (Elson *et al.*, 2020) and Statsmodmodels 0.12.2 (Seabold and Perktold, 2010) were used for the statistical analysis of the models and for creating linear regression models between data sets. For access to the code used, please refer to the author of this work.

2.1.3 Meteorological/Structural Property Data

All meteorological and structural property data used was obtained from the Copernicus Climate Data Store. The "ERA5-Land hourly data set from 1981 to present" was used (Muñoz Sabater, 2019). ERA5-Land corresponds to a reanalysis dataset that combines hourly model data and observed values on a global scale. The data set has a spatial resolution of 0.1° x 0.1° with a native resolution of 9 km. The basis of the ERA5-Land dataset is the Tiled ECMWF Scheme for Surface Exchanges over Land incorporating land surface hydrology (H-TESSEL) (ECMWF, 2018). To keep the amount of data to a manageable size, hourly data were downloaded only at 12:00, 13:00, and 14:00 for the whole timespan that SIF-Data (see chapter 2.1.3 in this work) was available (01 April 2018 to 31 July 2021). The downloaded parameters and their corresponding units can be seen in table 1. The hourly data from 12:00 to 14:00 were needed to calculate values for 13:30, corresponding to the time of the day of the available SIF-data.

Table 2 Data downloaded from the Copernicus CDS ERA5-Land hourly dataset from 1981 to present

Variable	Unit
10m u-component of wind (eastward)	ms^{-1}
10m v-component of wind (northward)	ms^{-1}
2m temperature	K
2m dewpoint temperature	K
Leaf area index, high vegetation	m^2m^{-2}
Leaf area index, low vegetation	m^2m^{-2}
Surface net solar radiation	Jm^{-2}
Surface pressure	Pa
Total evaporation	m of water equivalent

The eastward component of wind (u-component) and the northward component of wind (v-component) were combined to calculate the speed and direction of the horizontal wind at a height of 10m. The dewpoint temperature was used as a measure of the humidity in the air. The leaf area index (LAI) for low and high vegetation was needed to calculate the overall LAI over the whole vegetation.

2.1.4 Satellite Based Sun-Induced Chlorophyll Fluorescence

For this work, global SIF data from the TROPOspheric Monitoring Instrument (TROPOMI), the sensor of the Sentinel-5 Precursor Earth observation satellite, was used. This data was made available to the public via National Aeronautics and Space Administration's Jet Propulsion Laboratory (NASA JPL) (NASA, 2020). TROPOMI is able to measure the SIF signal in the approximate spectral range of 650-850 nm. Here, a global TROPOMI SIF data set at the wavelength 740 nm was used (for a more detailed description of the data see (Guanter *et al.*, 2021)). The data has a spatial resolution of 0.05° and is publicly available as a 16-day composite between 01.04.2018 and 31.07.2021 (Caltech TROPOMI SIF Data, 2021). The composite was created using the mean values of measurements during the 16-day interval. Negative SIF values were neglected for calculations, especially since they may originate from instrument noise or the retrieval assumption of a known shape of the fluorescence spectrum over vegetation, which is not applicable to non-vegetated areas (Wang *et al.*, 2021) and therefore set to voids.

2.2 Methods

2.2.1 Data Harmonization

In order to be able to compute the ERA5 data with the TROPOMI data, both data sets were reprojected to the same global coordinate system (WGS 84). After creating a subset of the global SIF data set with the same geographical extent as the ERA5 data (see 2.1.1 in this work), SIF data was aggregated to the same spatial resolution (0.1°) using the mean value of the original pixels. In addition, to match

the time of day of the SIF-measurements, values for 13:30 were calculated using the ERA5 data. Since radiation values of the ERA5 reanalysis are accumulated over the entire day, hourly values were calculated first and then the average was calculated between 13:00 and 14:00. Also, for the remaining variables, the average value was calculated between 13:00 and 14:00. The only exception was the wind components: To assure, that positive and negative values (in vector geometry plane) did not cancel each other out and/or would result in an underestimation of wind speed, only the wind components for 14:00 were considered. From all the ERA5 data variables 16-day composites were created matching the timesteps of the TROPOMI SIF data using the mean value over a 16-day interval.

2.2.2 Calculating ET for a Reference Model

The work presented here is based on the FAO standard model for calculating ET (Allen *et al.*, 1998), which in turn is based on the PM equation:

$$ET_0 = \frac{\Delta*(R_n-G)+\rho_a*C_p*\frac{(e_s-e_a)}{r_a}}{\Delta+\gamma*(1+\frac{r_s}{r_a})} \quad (2.1)$$

ET_0: Evapotranspiration [$\boldsymbol{mm\ d^{-1}}$]

R_n : Net radiation at the crop surface [$\boldsymbol{MJ\ m^{-2}\ d^{-1}}$]

G: Soil heat flux density [$\boldsymbol{MJ\ m^{-2}\ d^{-1}}$]

ρ_a: Mean air density at constant pressure [$\boldsymbol{kg\ m^{-3}}$]

C_p: Specific heat of air [$\boldsymbol{MJ\ kg^{-1}\ °C^{-1}}$]

r_a: Aerodynamic resistance [$\boldsymbol{s\ m^{-2}}$]

r_s: Stomatal resistance [$\boldsymbol{s\ m^{-2}}$]

u_2: Wind speed at 2m height [$\boldsymbol{m\ s^{-2}}$]

e_s: Saturation vapor pressure [***kPa***]

e_a: Actual vapor pressure [***kPa***]

e_s - e_a: Saturation vapor pressure deficit [***kPa***]

Δ : Slope of vapor pressure curve [$\boldsymbol{kPa\ °C^{-1}}$]

γ: Psychrometric constant [$\boldsymbol{kPa\ °C^{-1}}$]

Most of the variables in equation (2.1) needed to be estimated using further calculations. The reference model in this paper is based on the FAO guidebook (Allen *et al.*, 1998) and uses the provided values for the reference crop ET estimation therein. This simplification does not consider the predominant vegetation type but assumes a uniform crop height across the study site and time. With the data described in chapter 2.1.2 and the proposed values from the FAO guidebook, the following variables were calculated:

Table 3 Variables calculated using ERA5-Land meteorological/structural data

Relative Humidity	[%]
Ground Heat Flux	[MJ m^{-2} h^{-1}]
Vapor Pressure of Saturated Air	[kPa]
Actual Vapor Pressure	[kPa]
Vapor Pressure Deficit	[kPa]
Psychrometric Constant	[kPa °C^{-1}]
Slope of Vapor Pressure Curve	[kPa °C^{-1}]
Wind Speed at 2m Height	[m s^{-1}]
Aerodynamic Resistance	[s m^{-1}]
Surface Resistance	[s m^{-1}]

The relative humidity (RH) [%] at 13:30 was calculated using the relationship between the 2m temperature and the 2m dewpoint temperature:

$$RH = 100 * e^{\frac{c*b*(T_d - T)}{(c+T)*(c+T_d)}} \quad (2.2)$$

Where T_d is the 2m dewpoint temperature [°C], T is the 2m temperature [°C] and c is 243.04 and b corresponds to the value 17.625 (Alduchov and Eskridge, 1996).

The ground heat flux (G) [MJ m^{-2} h^{-1}] was approximated as 10% of the crop surface net radiation during daylight periods (R_n) [MJ m^{-2} h^{-1}].

The vapor pressure of saturated air (e_s) [kPa] was approximated using the 2m temperature:

$$e_s = e^0(T) \rightarrow e^0(T) = 0.6108 * e^{\frac{17.27*T}{T+273.3}} \quad (2.3)$$

For the calculation of the actual vapor pressure (e_a) [kPa], we used the relationship between the RH and e_s:

$$e_a = e_s * \frac{RH}{100} \quad (2.4)$$

Vapor pressure deficit (VPD) [kPa] was calculated as the difference between e_s and e_a.

The psychrometric constant (γ) [kPa°C^{-1}] was calculated using the specific heat of the air (C_p) [1.013*10^{-3} MJ°C^{-1}kg^{-1}], the atmospheric pressure (P) [kPa], the ratio of molecular weight of water vapor/dry air (ε = 0.622) [-] and the latent heat of vaporization (λ) [2.45 MJkg^{-1}]:

$$\gamma = \frac{C_p * P}{\varepsilon * \lambda} = \frac{1.013 * 10^{-3} * P}{0.622 * 2.45} = 0.6647 * 10^{-3} * P \quad (2.5)$$

The slope of the vapor pressure curve (Δ) was calculated using T [°C]:

$$\Delta = \frac{4098 * [0.6108 * e^{\left(\frac{17.27 * T}{T + 237.3}\right)}]}{(T + 237.3)^2} \quad (2.6)$$

As we needed the wind speed at 2m height (u_2), but ERA5-Land provided us with values for 10m height (u, v [ms^{-1}]), we calculated the wind speed/direction at 10m (equation 2.7) and translated the value down to a height of 2m (equation 2.8):

$$u_{10} = \sqrt{(u^2 v^2)} \quad (2.7)$$

$$u_2 = u_{10} * \frac{4.87}{\ln(678 - 5.42)} \quad (2.8)$$

Aerodynamic resistance (r_a) [sm^{-1}] was calculated based on the height of wind measurements (z_m) [m], the height of humidity measurements (z_h) [m], the zero displacement height (d) [m], the roughness length governing momentum transfer (z_{om}) [m], the roughness length governing transfer of heat and vapor (z_{oh}) [m], the Karman's constant (k) [-] and the wind speed at 2m height (u_2) [ms^{-1}]:

$$r_a = \frac{\ln(\frac{z_m - d}{z_{om}}) * \ln\frac{z_h - d}{z_{oh}}}{k^2 * u_z} \quad (2.9)$$

As the FAO reference crop ET model assumes a universal crop height (h_c) of 0.12m, the parameters d, z_{om} and z_{oh} were calculated using the formulas 2.10 to 2.12:

$$d = \frac{2}{3} * h_c \quad (2.10)$$

$$z_{om} = 0.123 * h_c \quad (2.11)$$

$$z_{oh} = 0.1 * z_{om} \quad (2.12)$$

The surface resistance (r_s) [sm^{-1}] was calculated from the stomatal resistance of a well-illuminated leaf (r_l) [100 sm^{-1}] and the active LAI (LAI_{active}) [m^{2}m^{-2}], which was approximated as 50% of the total LAI:

$$r_s = \frac{r_l}{LAI_{active}} \quad (2.13)$$

Using these values in the PM-equation proposed by the FAO, ET values were calculated over the whole timespan with a 16-day temporal resolution. The FAO reference crop ET model was then compared and evaluated with the ERA5-Land total evaporation data, which act here as a validation dataset. In a next step, individual variables of the reference PM equation were replaced by TROPOMI-SIF values.

2.2.3 Introducing Sun-Induced Chlorophyll Fluorescence to the Reference Model

A computationally efficient approach was chosen for the integration of SIF values into the FAO reference crop ET PM-equation in order not to exceed the computational and temporal limits of this master's thesis. A linear regression model was fitted between the SIF values and one of the variables contained in the PM equation at a time. The linear regression equation was then used to stretch the SIF values to an appropriate range of values to replace the initial variable in the equation. Utilized were linear models between:

Table 4 Built linear models to replace the variables by SIF values

Nr.	Linear regression model	Coefficient m	Intercept q
1.	SIF & ET	0.6895	0.1778
2.	SIF & R_n	0.3934	0.1305
3.	SIF & LAI	0.1415	0.0525
4.	SIF & LAI_{active}	0.2830	0.0525
5.	SIF & r_s	-0.0018	0.7614
6.	SIF & r_s*$VPD^{0.5}$	-0.0008	0.6936

Lu et al (2018) examined in their study, whether SIF values can be used to accurately estimate T. They found that SIF has a generally positive linear correlation with T. Only under stress situations does SIF show a non-linearity with T. As T is the main component of terrestrial ET (Schlesinger and Jasechko, 2014), we investigated whether ET can be directly approximated by SIF using a linear relation.

As radiation is the main driving source of SIF and R_n is highly correlated with SIF (Ma *et al.*, 2022), we further replaced R_n with linearly stretched SIF values.

While the existing FAO approach allows estimating potential ET only, based on the greenness of plants, we tried to replace the biological drivers such as LAI and r_s by SIF to move closer to an estimation of actual ET (Damm, Roethlin and Fritsche, 2018).

Shan *et al.* (2021) have also shown a high correlation between SIF and canopy conductance*$VPD^{0.5}$ in their study, which is why we finally created a model in which SIF values were stretched to the

range of r_s*$VPD^{0.5}$ using a linear regression function, and then a new r_s was calculated and inserted into the PM equation.

The linear regression models (equation 2.14) were used to scale each of the SIF values to an adequate range of values to substitute for the variable being replaced:

$$SIF = m * x + q \quad (2.14)$$

Where x is the variable to be replaced in the PM equation, m is the linear regression coefficient and q is the linear regression intercept.

3. Results

The FAO reference model showed on average higher values compared to the validation data of ERA5. While the ERA5 total evaporation data showed a mean value of 0.14 mm h^{-1} over the whole timespan, the FAO reference approach provided a mean ET value of 0.54 mm h^{-1}. To compensate for this bias, all values of the reference model, as well as those of the derived SIF models, were divided by a factor of four to approximate the ERA5-Total evaporation validation data.

In some cases, the models still showed excessive values even after bias correction. The values for the SIF-ET model and the SIF-R_n model were particularly high. After bias correction, for the SIF-ET model we still obtained maximum values of up to 2.03 mm h^{-1} with an average of 0.22 mm h^{-1} and for the SIF-R_n model maximum values of up to 1.76 mm h^{-1} with an average of 0.24 mm h^{-1}.

Statistics summarized in table 5 indicate the FAO reference model, after bias-correction, to be in a similar range of values as the ERA5 total evaporation data. The two models in which the LAI respectively LAI_{active} was replaced by SIF show the same characteristic values. The models in which we approximated r_s by SIF are also in an acceptable range of values, but underestimate ET by about 0.02 mm h^{-1} for the SIF-r_s model and 0.05 mm h^{-1} for the SIF-r_s*$VPD^{0.5}$ model.

Missing values in individual models are due to negative and/or not available SIF values, which were excluded in the calculations. Furthermore, with the calculation method used, we obtained strongly negative values for r_s due to a negative regression coefficient for the SIF-r_s and SIF-r_s*VPD^{05} models. These were also replaced by voids. Therefore, the SIF-r_s and SIF-R_s*$VPD^{0.5}$ models showed missing values in large parts of northern and central Europe.

Table 5 Characteristic ET values [mm h^{-1}] for the different models after bias-correction

Model	Min	Max	Mean	Median
ERA5 Validation	-0.0602	0.6931	0.1413	0.1133
Reference	0.0000	0.5607	0.1361	0.1254
SIF-ET	0.0000	2.0289	0.2173	0.1562
SIF-R_n	-0.0577	1.7550	0.2356	0.1568
SIF-LAI	0.0000	0.5461	0.1655	0.1658
SIF-LAI_{active}	0.0000	0.5461	0.1655	0.1658
SIF-r_s	0.0004	0.5540	0.1197	0.1005
SIF-r_s*$VPD^{0.5}$	0.0000	0.5541	0.0959	0.0676

3.1 Timeseries Comparison Across Different Sites/Landcover Classes

In all models, we recognize a typical course of the phenological cycle, in which the growth phase begins in spring, maximum activity is reached in summer, and vegetation activity declines during autumn (Khaliq, Peroni and Chiaberge, 2018).

Even after bias-correction, the models differ strongly from each other. Particularly striking are those models in which SIF values were used directly as a proxy for ET and R_n, respectively. Fewer outliers were achieved, when SIF values were used for less weighted components of the PM equation (i.e. LAI_{active} and r_s). In figure 2 only the models are shown, which have no or only few gaps. A complete compilation of the calculated models can be found in the appendix. Due to the calculation method used, large gaps were found especially in the northern regions, where we partly had no SIF data, or found negative values which were neglected for further calculations. Furthermore, for the SIF-r_s and SIF-r_s*$VPD^{0.5}$ models we discarded strongly negative values also in large parts of central Europe, which is why they were excluded from the time-series analysis.

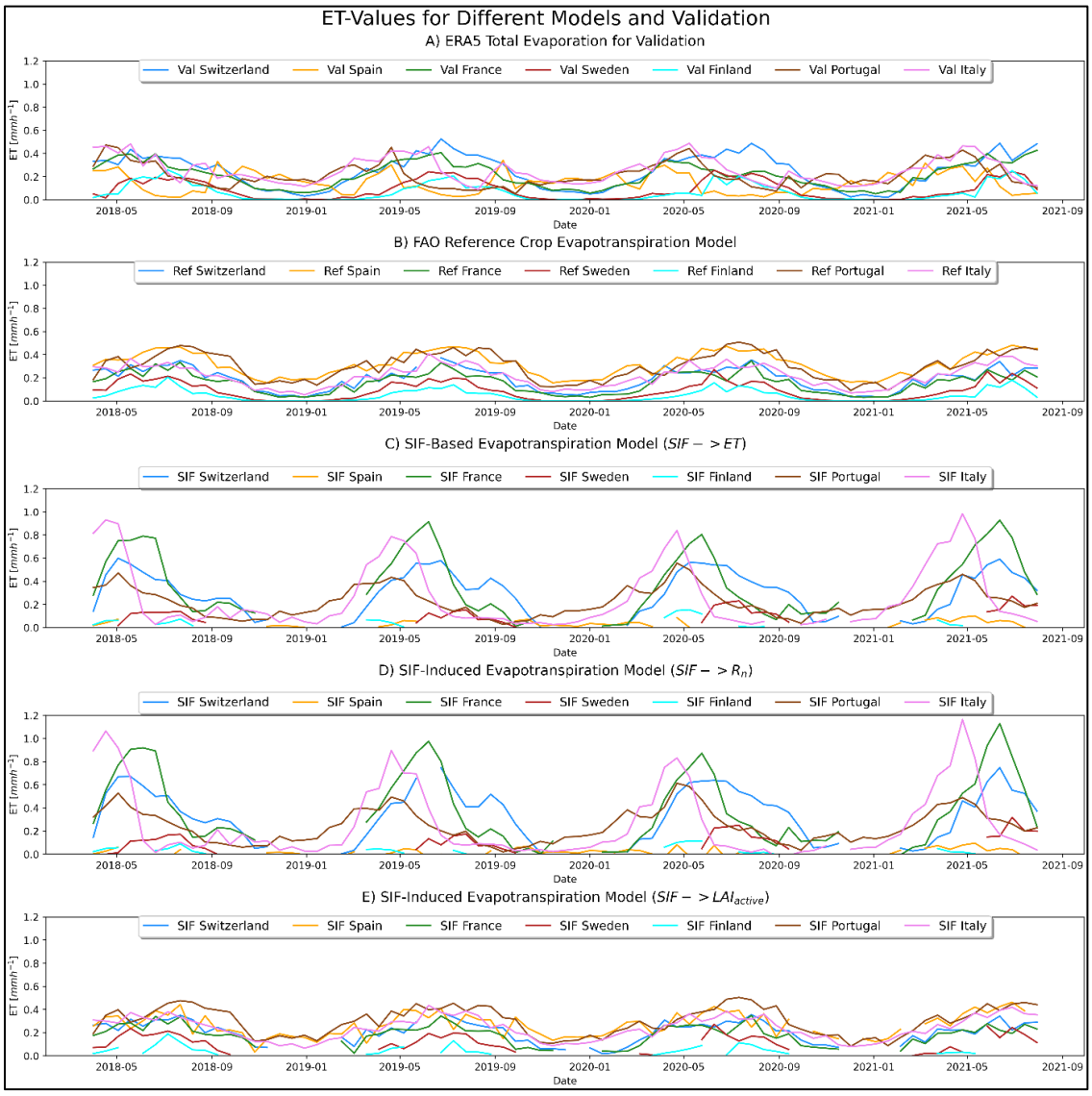

Figure 2 Subplots of the ERA5 validation, the FAO reference crop and the SIF-based models over the whole timespan from 01.04.2018 to 30.07.2021 in a 16d-interval. A) ERA5 total evaporation, B) FAO reference crop ET model, C) SIF-ET model, D) SIF-R_n model, E) SIF-LAI_{active} model

Figure 2 shows the timeseries of ET values based on the different modelling algorithms and the validation dataset for different sites and landcover classes. The two topmost plots indicate the ET timeseries as found in the validation and reference data set. Subplot 2A) shows the timeseries at corresponding sites based on the ERA5-total evaporation data. This plot will indicate the validation data. Generally, it indicates highest values in densely vegetated areas such as forest and agricultural fields (up to 0.6 mmh^{-1}). Lowest ET values are found in sites located in Scandinavia. In subplot 2B) the ET values are displayed, when using the FAO reference crop ET model. The timeseries is used as a reference model to inspect deviations resulting from the insertion of the SIF values. Highest ET values (up to 0.5mmh^{-1}) are found in Spain (desert) and Portugal (mixed species forest and agricultural fields). Nordic countries (Finland with grassland and shrubs, Sweden with coniferous forest and grassland) indicate lowest values reaching a max. ET of around 0.2 mmh^{-1}. In both the validation and the reference model the season of Scandinavian countries are shorter (length of growing season (LGS) around 180 days) and later in season (start in late April), when compared to sites in lower altitudes (LGS around 270 days and start of season in February-March).

Figure 2 also contains three of the resulting timeseries of the computed SIF-based approaches performed in this thesis, namely the SIF-approaches based on C) ET, D) R_n and E) LAI_{active}. The model based on ET and R_n feature similar characteristics, including ET values of up to 1.0 and 1.2 mmh^{-1}, respectively, for the locations in both France and Sicily (both sites dominated by agricultural landcover). Both these locations further show a clear peak in ET values at the start of season with Sicily being earlier in season than France. Both timeseries feature large gaps in the dataset over Sweden, Finland and Spain. Overall, the lowest ET Values are found in the study site situated in the desert in Spain with max. ET values of 0.1 mmh^{-1} in both models. The approach based on SIF for LAI_{active} (figure 2E)) results in SIF values across all test sites between 0 to below 0.5 mmh^{-1}. All sites follow a similar trend using this approach, with highest values found in the site in Portugal and lowest in the area of Finland. Also, in this timeseries large data gaps are included especially for sites in high latitudes. These missing values are due to negative and/or not available SIF values, which were excluded in the calculations. Negative SIF-Values after stretching the values according to chapter 2.2.3 were also discarded.

When comparing the validation data (figure 2A) with the results from the FAO reference approach (figure2B), the reference model indicates a smoother annual course and thus shows fewer peaks than the ERA5 total evaporation data. Discrepancies between the reference and the SIF based models (ET and R_n) are found for one in the test site in the Spanish desert. Where the ET values for the reference model are ranging to up to 0.5mmh^{-1}. A difference in trend can further be found between the reference and the two SIF-based approaches for those areas, where the SIF-based approaches indicate a peak of season.

Comparing the reference model (figure 2B) with the two SIF-based models, where SIF was used directly as a proxy for ET or R_n, the sites in France (Amiens) and Italy (Sicily), and to a lesser extent

the area in Switzerland (Laegern), show significant outliers in late spring and summer. While models 2C) and 2D) show large variation in values, model 2E) closely approximates the FAO reference model and thus shows less fluctuation over the course of the timeseries.

3.2 FAO-Reference-Model Compared to ERA5 Total Evaporation Validation Data

For comparison and checking for plausibility of the different models, 19 test locations were selected along the northern edge of the central European mainland (see figure 3). These range from Spain (Salamanca) to Latvia (Saldus Parish).

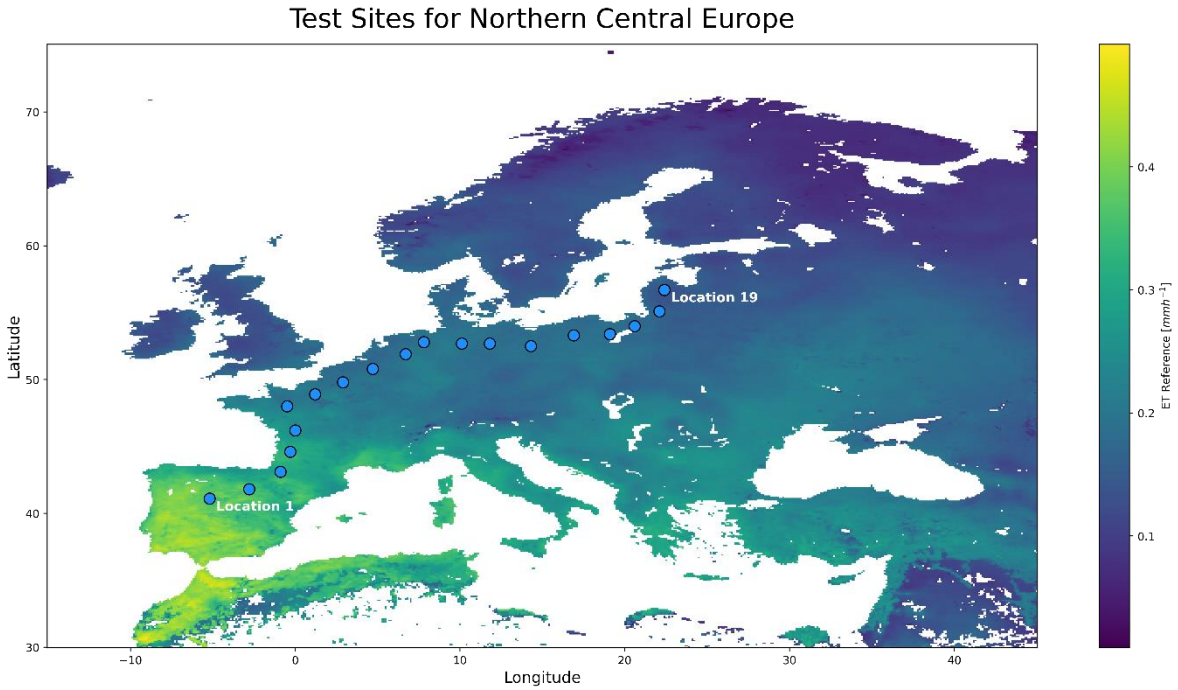

Figure 3 Location of the 19 test sites in northern Central Europe; in the background: ET values calculated based on the FAO reference approach for the 23.08.2018

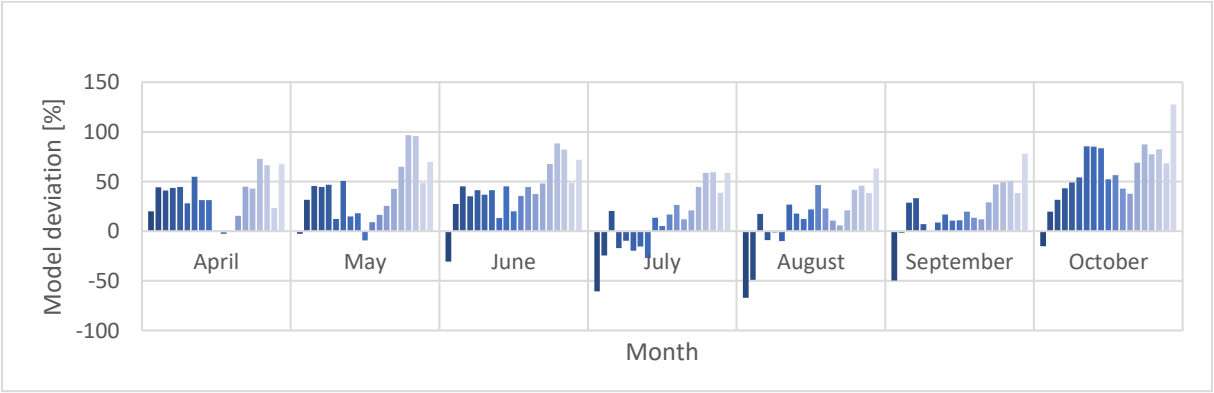

Figure 4 Deviation of ERA5-Total evaporation validation data from the calculated FAO reference approach in 2020 for the test pin locations indicated in figure 3

Figure 4 shows the model deviation for the selected test sites across northern Central Europe between the ERA5 total evaporation validation data and the calculated FAO reference approach over the growing season 2020. The same analysis was performed for the seasons 2018 and 2019. Largest

discrepancies of up to 100% are generally found in the locations of higher latitudes (sites No. 16-19). This indicates the reference model based on FAO to have lower ET values than the ERA5 validation data. Strongest negative values (down to -67%) indicating the opposite (lower values in ERA5 than in FAO based approach) are found in summer months (June – September) in the regions characterized by the lowest latitude.

Table 6 summarizes the mean model deviation results across the three analyzed seasons. For 2018, we find an average deviation of the two models (ERA5 total evaporation and FAO reference model) of 18.00% and a median deviation of 20.63%. This implies that the validation data are about 18% higher than the FAO reference model data for the selected test sites. In 2019, the deviation is even slightly higher with an average of 29.82% as well as a median deviation of 35.08%. For 2020, the average deviation is 31.46% and the median deviation is 33.37%.

Table 6 Deviation of ERA5 total evaporation data compared to calculated data from FAO reference model

Year	Mean Dev. [%]	Median Dev. [%]
2018	17.998	20.625
2019	29.821	35.076
2020	31.464	33.368
All	**26.428**	**29.838**

Thus, we see that after the bias-correction the ERA5 validation data for the selected test sites from April to October is on average about 26% higher than the calculated data using the FAO reference approach. In the further comparison, however, we are mainly interested in the quality of the different SIF-based models and whether they are able to show stress situations for vegetation better than the reference model.

3.3 SIF-Based Models Statistically Compared to FAO-Reference-Model

To investigate how well the different SIF-based models correlate with the reference approach, they were plotted against the reference model and a linear regression was fitted through the data (see Appendix for plots) resulting in a linear regression coefficient and regression intercept (see chapter 2.2.3). In addition, the coefficient of determination (R^2) and the root mean squared error (RMSE) were calculated. R^2 gives us information about the strength of the relationship between the two data sets, while the RMSE describes the extent of the deviation of the data from each other.

Table 7 shows the achieved results of the statistical evaluation of the different SIF-based models computed for this thesis against the FAO reference crop ET model. Highest cross-correlation values were found between reference and SIF-LAI_{active} and SIF-r_s (0.911), while lowest values are found between reference and SIF-ET (0.15). Correspondingly, the root mean squared error is lowest for reference and SIF-LAI_{active} (0.031) and SIF-r_s (0.038), and highest for the reference and SIF-ET

combination (0.219). With the RMSE of SIF-LAI_{active} being even lower than SIF-r_s, this indicates SIF-LAI_{active} to be the best fit.

Table 7 Statistical comparison between the FAO-reference model and the ERA5 validation data and between the FAO reference approach and each of the calculated SIF-based models in this thesis. The linear regression coefficient and the regression intercept are provided to describe the slope of the linear regression line

Reference compared to:	R^2	RMSE	Coefficient	Intercept
Validation	0.501	0.091	0.8304	0.0377
SIF-ET	0.150	0.188	0.8576	0.0673
SIF-R_n	0.187	0.219	1.1069	0.0341
SIF-LAI_{act}	0.911	0.031	1.0000	-0.0087
SIF-r_s	0.911	0.038	0.8648	-0.0063
SIF-$r_s VPD^{0.5}$	0.843	0.060	0.8300	-0.0238

3.4 Plausibility Check Regarding Plant Stress Situations

As Europe was severely affected by a combined drought and heat wave in the year 2018 (Ahmed *et al.*, 2020), this year was selected to examine how our values differ from the FAO reference approach to the SIF-based models regarding the vegetation stress situations. In their paper, Ahmed *et al.* (2020) state that the ET values for April 2018 were close to their long-term baseline, with only some areas in central and eastern Europe showing higher than normal ET, which may have been caused by warmer spring conditions. Based on these findings, we used the month of April of our FAO reference approach model as a reference and calculated the deviation of our models from this data set for each month.

Using the ERA5-total evaporation validation data, we can see the progression that the data should theoretically show over the year (figure 5). From April to May we find a general increase of ET values over all test sites, especially strong is the increase in the northeast of Central Europe (up to 80%). In June, the first values in Central Europe start to fall below the April values. This trend continues in July, while from August to October almost everywhere, except for sites 3, 15 and 16, the values drop below the April values (down to -76%).

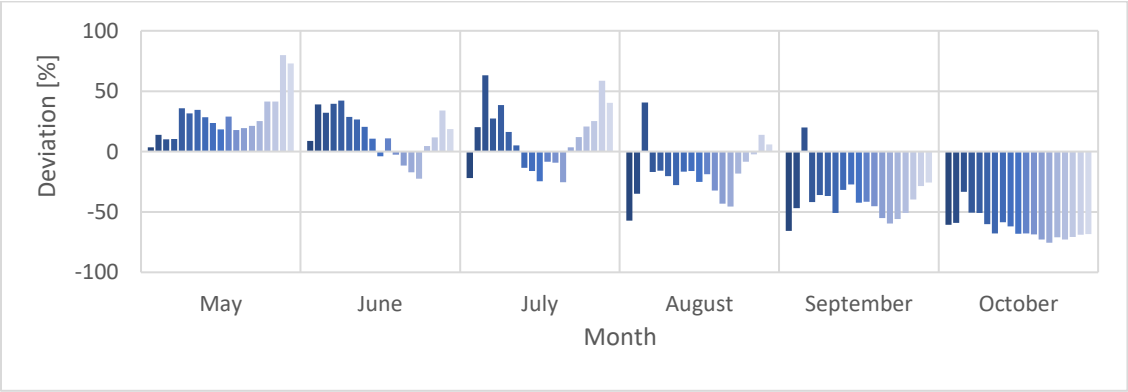

Figure 5 ERA5 total evaporation: In-season comparison of the trend between the reference month April versus the remaining months. From left to right for each month: Site of interest 1 -19

Figure 6 further indicates a deviation over the progression over the year between the FAO-based approach to the validation data. We can see, that for our interest sites along the northern edge of Central Europe, the progression over the year deviates from the validation data. On the whole, we see a similar pattern, but with some variations especially in the months of July, August and September.

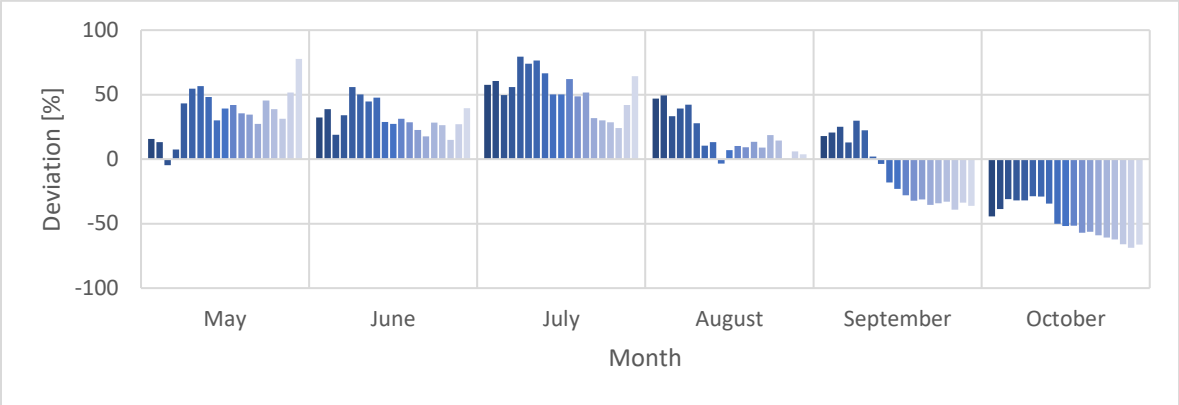

Figure 6 FAO reference approach model: In-season comparison of the trend between the reference month April versus the remaining months. From left to right for each month: Site of interest 1-19

While in the validation data we can already see a decrease in ET values for Central Europe in June, which has further intensified and expanded in the following months, this decrease in values compared to the April data in the FAO model is only visible in August, September and October.
However, in order to check whether we can better approximate the actual seasonal trend by integrating SIF values into the PM equation, we compare the values of the reference model and our SIF-based models.

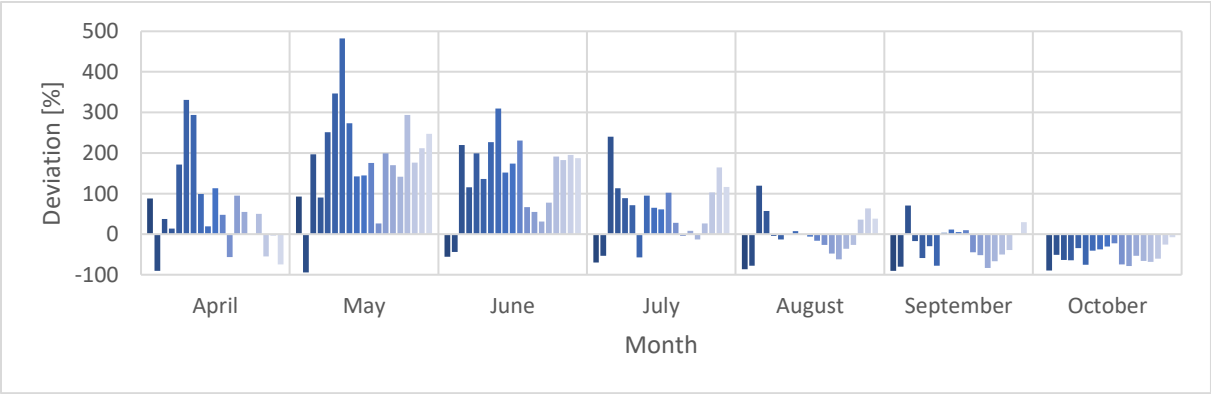

Figure 7 SIF-ET Model: In-season comparison of the trend between the reference month April from the FAO-reference approach versus the season for the SIF-ET model. From left to right for each month: Site of interest 1-19

Figure 7 shows the deviation of the ET values of the SIF-ET model compared to the month April of the FAO reference approach. It is striking that we find strong overestimations of the values in the months April to July (up to 482% in the month of May). Furthermore, we find an underestimation in the westernmost test sites throughout the season (up to -94%). While the FAO reference model still shows a predominantly positive deviation in August, the SIF-ET model already shows a large-scale decrease of ET values over central Europe.

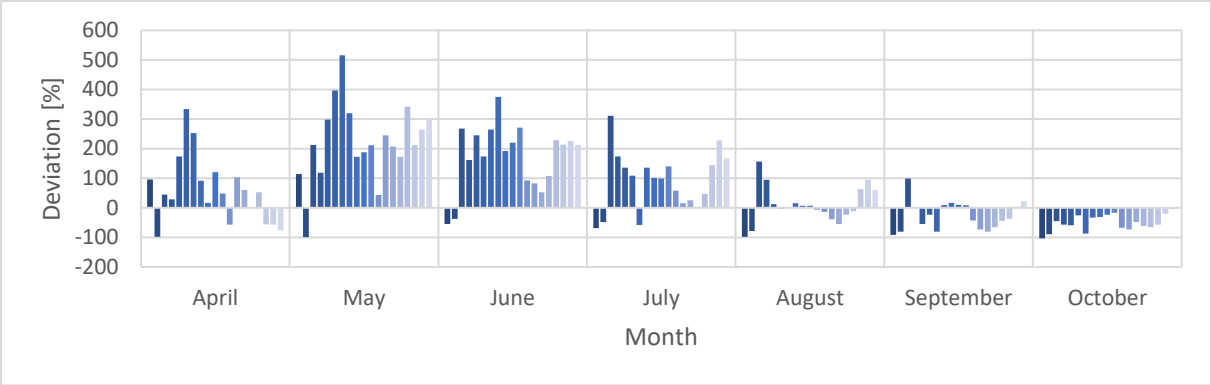

Figure 8 SIF-Rn Model: In-season comparison of the trend between the reference month April from the FAO-reference approach versus the season for the SIF-Rn model. From left to right for each month: Site of interest 1-19

The deviations between the month April of the FAO reference model to the SIF-R_n model shows a very similar pattern (figure 8) as the FAO reference approach to the SIF-ET model. It is remarkable that we find even higher deviations (up to 516%, and down to -99%).

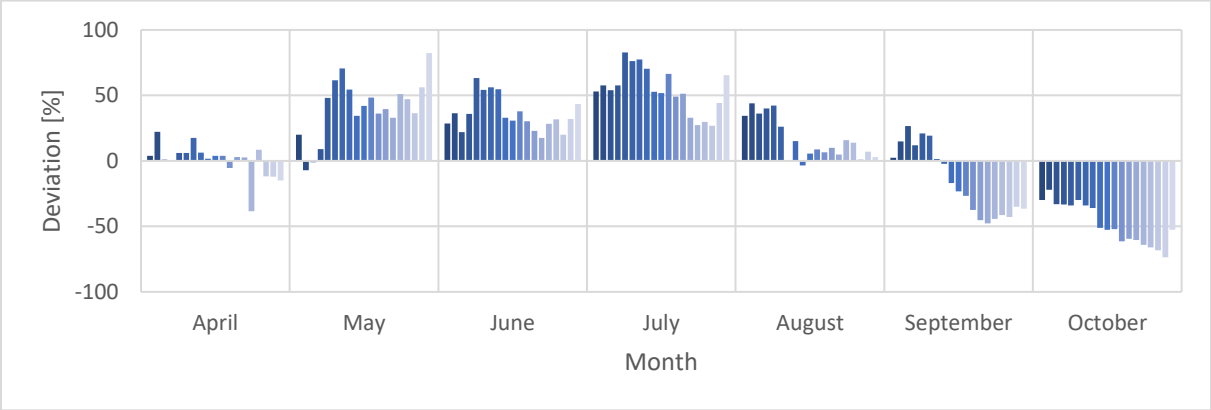

Figure 9 SIF-LAI_{active} Model: In-season comparison of the trend between the reference month April from the FAO-reference approach versus the season for the SIF-LAI_{active} model. From left to right for each month: Site of interest 1-19

In figure 9 we compare the SIF-LAI_{active} model to the month April of the FAO reference model. Compared to the SIF-ET and SIF-R_n model, we are again closer to the course of the FAO reference approach. However, it is striking that we already find a negative deviation of up to -38% in the month of April. These underestimations in April are mainly found in eastern Central Europe. In the months of May, June and July we find predominantly positive deviations (of up to 83%) until in August a first break in the values is observed in Central Europe, which then manifests itself in September, especially in the eastern test sites, and in October a break in the values is recorded across all test sites with deviations down to -74%.

4. Discussion

There are many uncertainties associated with the calculation of ET using the FAO reference crop approach. For one, the PM equation is very complex and requires many meteorological and biophysiological inputs, all of which are subject to uncertainties in measurements and/or estimations. In addition, this method assumes that we have a uniform land surface across the study site and time, namely a hypothetical crop with a height of 0.12 m and a bulk surface resistance of 70 sm^{-1} (Allen *et al.*, 1998). These may be possible reasons why our reference model showed highly overpredicted values compared to the ERA5 total evaporation validation data and could explain the bias factor found. The ERA5 total evaporation showed to be a reliable estimation of ET when compared to the findings of Ahmed *et al.* (Ahmed *et al.*, 2021), therefore it seemed suitable to be used as a validation data set.

4.1 FAO Reference Crop ET Model

While the statistical values of the FAO reference approach suggest that we achieved a reliable approximation to the ERA5 validation data (table 5), we notice some differences when comparing the time series of the two models (figure 2A/2B). For the study site in the Spanish desert, the ERA5 validation data show a clear pattern that ET values reach their maximum (ca. 0.4 mmh^{-1}) especially in spring, while hardly any ET was measured in summer (less than 0.1 mmh^{-1}) and a peak in ET is seen again in autumn 2018 and 2019. In the FAO reference model, on the other hand, the Spanish desert, along with the Portuguese forest- and agricultural lands, has the highest values (up to about 0.6 mmh^{-1}) and shows a typical phenological cycle, with an increase of ET values in spring, a maximum in summer, a weakening in autumn to a minimum in winter. This behavior can be linked to the applied computational method, which assumed universal vegetation cover across the study site. Making the result solemnly dependent on the meteorological data. We thus recognize in the FAO reference model mainly the geographical location of the different sites. While in the more southern regions like Spain, Portugal, Italy and up to Switzerland more solar energy as well as higher temperatures over a longer period of time are available, the Scandinavian sites are characterized by much lower temperatures and the length of time where enough solar energy is provided for to lead to ET is far shorter (see figure 2). Therefore, we have hardly any ET from around October to March in these sites.

While the statistical values of the FAO reference approach suggest that we achieved a good approximation to the ERA5 validation data (table 5), we notice some differences when looking at the time series of the two models (figure 2A/2B). For the study site in the Spanish desert, the ERA5 validation data show a clear pattern that ET values reach their maximum (ca. 0.4 mmh-1) especially in spring, while hardly any ET was measured in summer (less than 0.1 mmh-1) and a peak in ET is seen again in autumn 2018 and 2019. In the FAO reference model, on the other hand, the Spanish desert, along with the Portuguese forest- and agricultural lands, has the highest values (up to about

0.6 mmh^{-1}) and shows a typical phenological cycle, with an increase of ET values in spring, a maximum in summer, a weakening in autumn to a minimum in winter. However, this makes perfect sense when we consider our computational method, which assumed universal vegetation cover across the study site. This meant that we were really only dependent on the meteorological data. We thus recognize in the FAO reference model mainly the geographical location of the different sites. While in the more southern regions like Spain, Portugal, Italy and up to Switzerland we have more solar energy and higher temperatures over a longer period of time, in the Scandinavian sites we have much lower temperatures and only during a shorter period of time enough solar energy to run ET. Therefore, we have hardly any ET from around October to March.

4.2 Introduction of SIF to the FAO Reference Approach

Our SIF-ET model as well as the SIF-R_n model indicated weakest correlation to the FAO reference model with R^2 values of 0.150 and 0.187, respectively, which indicates that even after stretching the SIF values to the parameter range, the usage of SIF for these parameters lead to a too diverse range of values. This finding displayed in table 7 implies that we tried to approximate a rather non-linear relationship using a linear regression. Furthermore, from this, we could deduce that R_n is heavily weighted in the PM equation and thus has a large impact on the final result of the model equation. If we replace ET directly with a linearly stretched SIF, we obtain a larger range of values and thus overestimate ET, indicating again, that the relationship between ET and SIF might not be linear. Estimating ET directly from SIF resulted in a low correlation with the reference ET data, consistent with findings by Damm *et al.* (2021) who also reported the lowest agreement between measured and modelled transpiration by using a linear function of SIF to approximate transpiration.

For the remaining SIF-based models, we found much higher correlations with the FAO reference model (an R^2 of 0.911 for SIF-LAI_{active} as well as SIF-r_s and an R^2 of 0.843 for SIF-r_s*$VPD^{0.5}$, see table 7). This indicates that the replaced parameters were weighted lighter in the overall equation. Accordingly, despite adjusting the parameter values, we obtained a reliable representation of the FAO reference ET model. However, caution should be applied when interpreting the SIF-r_s and SIF-r_s*$VPD^{0.5}$ models (see table 4): The models also resulted in strongly negative values over large parts of Europe for the stretched SIF due to the negative linear regression coefficients. These were discharged and not further considered leading to large gaps of data throughout the entire study site.

To examine whether our SIF-based models were better able to represent reduced ET values affected by heat and/or drought waves (Tsakiris and Vangelis, 2005) we compared the spatiotemporal deviation of our models relative to the month of April 2018 of the FAO reference model. The ERA5 total evaporation data agreed well with the findings of Ahmed *et al.* (2021) and was therefore used as a validation dataset showing how the variations in ET values differed from April 2018 across the season. Already in June 2018, we noticed the first negative deviations over Central Europe, which means that we found a decrease in ET values compared to the month of April. These negative

deviations manifested and propagated further towards the west in the month of July. In August, all but the test sites in the far east and one test site west of the Pyrenees had ET values below those of April, showing well the influence of the combined heat and drought wave during the year 2018. In September, only the test site west of the Pyrenees showed a positive ET deviation, while the rest of the sites indicated strongly negative deviations (on average -42%). Finally, in October, all ET values were below April, with a more pronounced deviation in Eastern Europe (-70%) than in Western Europe (-51%).

Compared to the course of the validation data, our model based on the FAO reference crop ET method showed a similar course over the whole year, but large deviations within the individual months (see figure 6). While we could observe the spread of the combined heat and drought wave from east to west already in June based on the validation data, this development is visible in the FAO reference approach only from August on, where we still find an increase of ET values in the west, first negative deviations in central Europe and only a weak increase in the east. The pattern becomes clearer in September, where we find a significant decrease in ET values in the East, while we still had an increase in the West. Then for the month of October we found a similar pattern as in the validation data. Higher deviation values are found in the East (67%) than in the West (38%).

The SIF-ET model provided a wide range of deviations from the month of April of the FAO Reference approach (from -94% up to 482%). For April we found negative deviation from -91% in the test location 2 in Spain up to 331% for the test site 6 in northern France (see figure 3). In the very East, our model produced lower values than the FAO approach. In May, we found a negative deviation only in test location 2, while everywhere else an increase of about 200% on average was seen. For the remaining months we found a negative deviation especially in Spain, while in western France we still had an increase in ET values. From July onwards, the heat and drought wave slowly made itself noticeable in Central Europe, which then extended further east and west in the following months.

The SIF-R_n model showed the same pattern as the SIF-ET model, except that the deviations were even more pronounced (from -99% to 516%). This may indicate that ET has a strong correlation with R_n, especially since both models showed the same pattern after SIF was introduced. This finding supports previously conducted studies by Heck *et al.* (2020) and Irmak *et al.* (2003).

The SIF-LAI_{active} model showed a very similar course as the FAO reference model but showed an underestimation of the ET values already in April in Eastern Europe (see figure 9). Also, in this model we find first signs of a heat and drought wave only in August, which then propagated eastward in September and produced negative deviations across all test sites in October.

4.3 Limitations of this study

The FAO reference crop ET estimation assumes a uniform vegetation cover for the entire study site, an assumption which cannot hold over a continental-wide test site. As our research environment is a highly dynamic and diverse landscape, this approach can only give an approximation of the actual

values for ET. Since the ERA5 reanalysis dataset also contains modeled values, it must be assumed that multiple uncertainties influence this dataset. This includes, for example, an assumption of a constant LAI (value of 3 m^2m^{-2}) for the study site in the Spanish desert, thereby not reflecting reality. Despite a computationally efficient approach, the models regularly overloaded the computational capacity of the PC system used, therefore we had to break the models into smaller and smaller pieces to avoid overloading the computer. Significantly more computing power would be needed to create more accurate models including more detailed data.

5. Conclusion

Remote sensing technologies offer a promising approach to help increasing the understanding of environmental variables such as ET by providing increased spatiotemporal coverage. However, the implementation of such data to accurately reflect the complex system of vegetation activity still faces substantial challenges. In this thesis, we created and assessed the applicability of several spaceborne SIF-based ET models. Some of the here presented SIF-based models for ET estimation on continental-coverage come close to the values of the FAO reference crop ET models and in general feature a reasonable seasonal cycle across diverse landcover classes and latitudes. Weakest correlation towards FAO reference across the diverse landcover classes was found for the substitution of SIF for ET and R_n. Best results, when compared to the FAO reference, were achieved by the SIF-LAI_{active} model. Our results further indicate a high correlation between R_n and ET. Generally, we conclude that the assumption of a linear correlation between SIF and various parameters of the PM equation is not capable of improving FAO reference crop model as the link is more complex than a linear relationship can reflect. In order to move from estimating potential ET closer to an estimation of actual ET, we recommend further studies to use modeling approaches, which take into account the non-linear correlations between the different parameters. In addition, we recommend using a land cover classification as a base to incorporate various vegetation-specific parameters into the model, to determine the actual ET values more precisely over a large study site.

Appendix

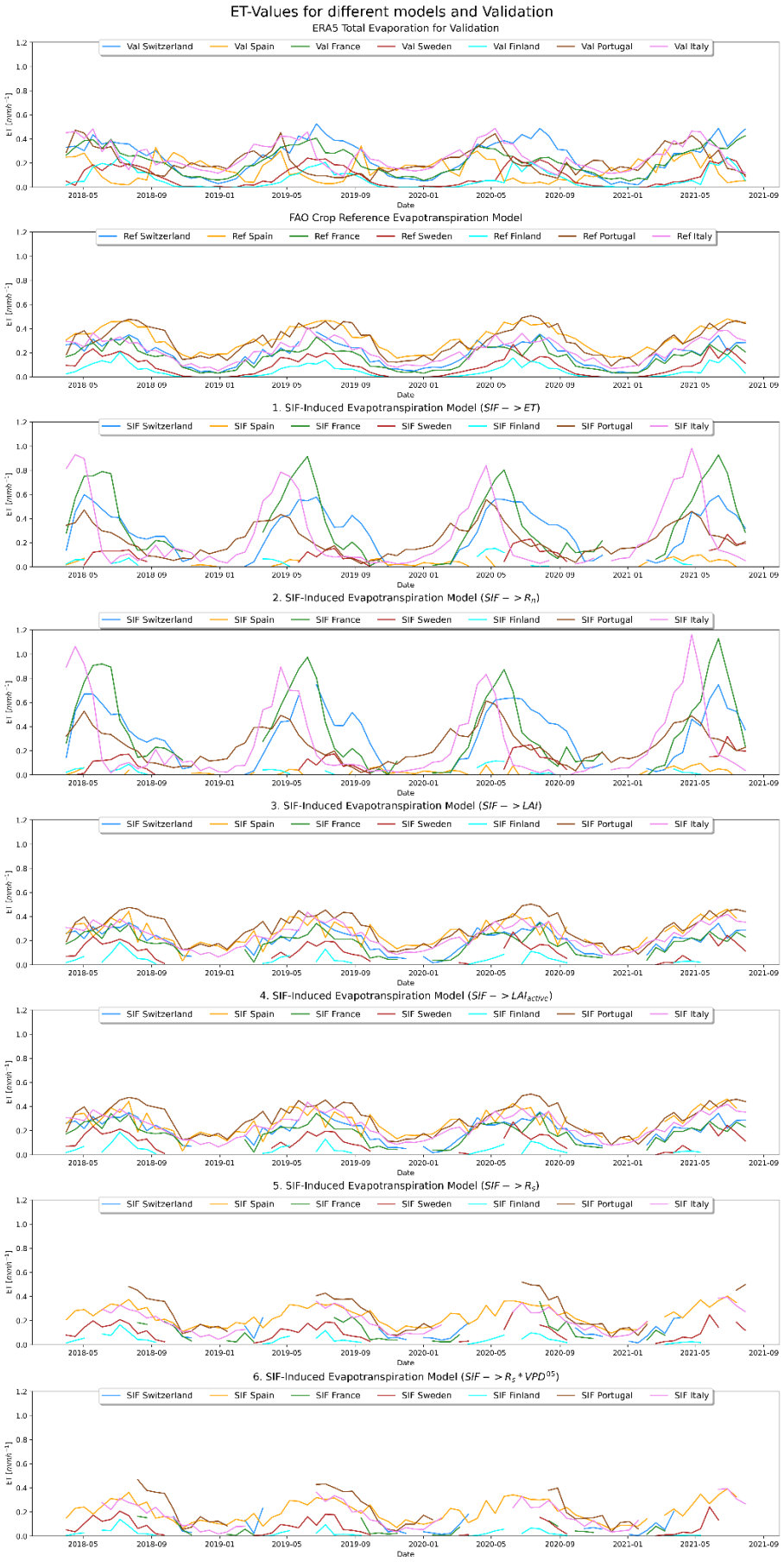

Figure 10 ET timeseries for all the models conducted in this thesis

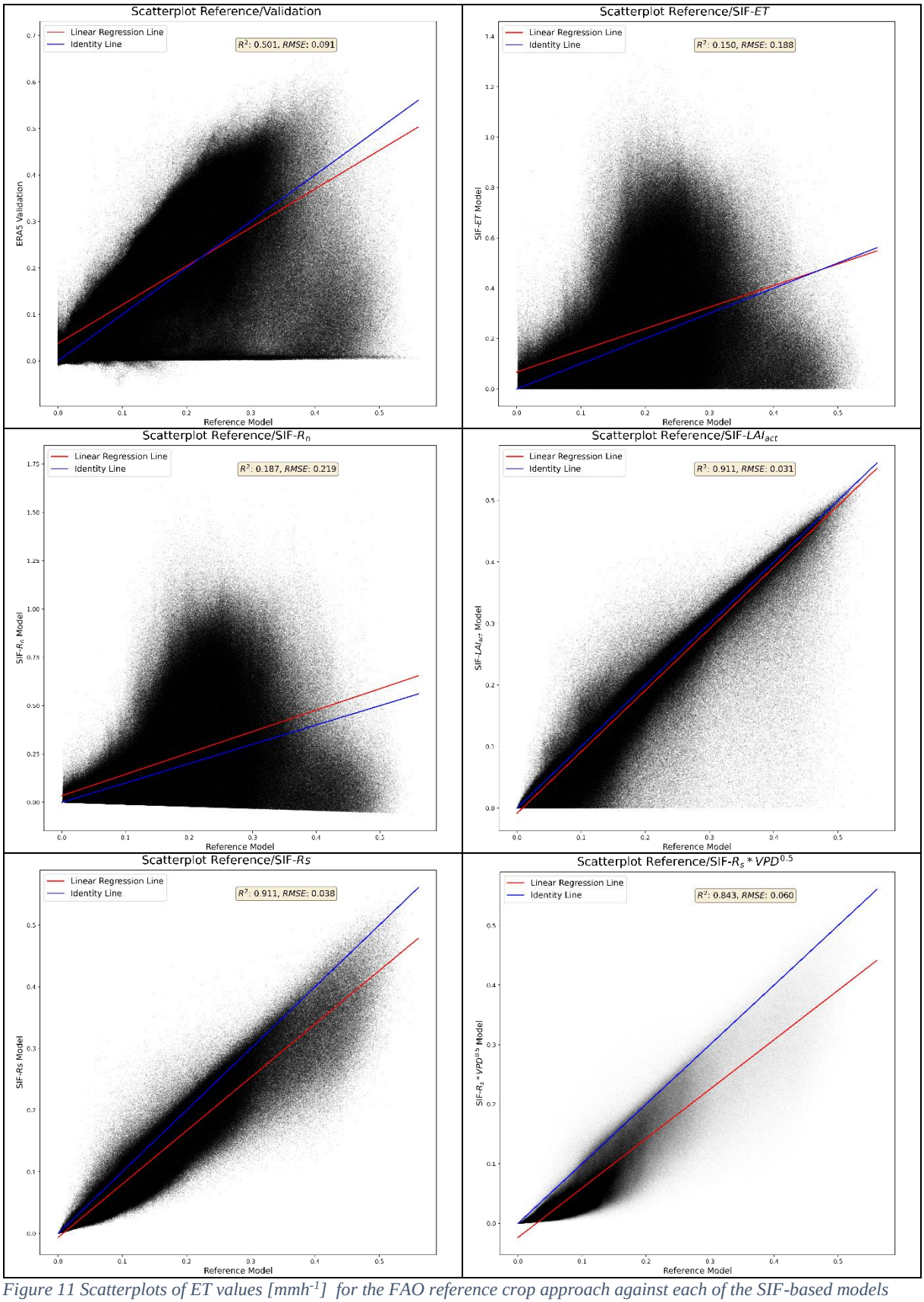

Figure 11 Scatterplots of ET values [mmh^{-1}] for the FAO reference crop approach against each of the SIF-based models

References

Ahmed, K.R. *et al.* (2021) 'A first assessment of the 2018 European drought impact on ecosystem evapotranspiration', *Remote Sensing*, 13(1), pp. 1–17. Available at: https://doi.org/10.3390/rs13010016.

Alduchov, O.A. and Eskridge, R.E. (1996) 'Improved Magnus Form Approximation of Saturation Vapor Pressure', *Journal of Applied Meteorology*, 35.

Allen, R.G. *et al.* (1998) *Crop evapotranspiration - Guidelines for computing crop water requirements - FAO Irrigation and drainage paper 56*. Rome. Available at: https://www.fao.org/3/x0490e/x0490e00.htm#Contents (Accessed: 14 March 2022).

Allen, R.G. *et al.* (2006) 'A recommendation on standardized surface resistance for hourly calculation of reference ETo by the FAO56 Penman-Monteith method', *Agricultural Water Management*, 81(1–2), pp. 1–22. Available at: https://doi.org/10.1016/j.agwat.2005.03.007.

Amatya, D.M. *et al.* (2016) 'Ecosystem evapotranspiration: Challenges in measurements, estimates, and modeling', *Transactions of the ASABE*, 59(2), pp. 555–560. Available at: https://doi.org/10.13031/trans.59.11808.

Anderson, M.C. *et al.* (2011) 'Mapping daily evapotranspiration at field to continental scales using geostationary and polar orbiting satellite imagery', *Hydrology and Earth System Sciences*, 15(1), pp. 223–239. Available at: https://doi.org/10.5194/hess-15-223-2011.

Barcza, Z. *et al.* (2009) 'Spatial representativeness of tall tower eddy covariance measurements using remote sensing and footprint analysis', *Agricultural and Forest Meteorology*, 149(5), pp. 795–807. Available at: https://doi.org/10.1016/j.agrformet.2008.10.021.

Bento-Gonçalves, A. *et al.* (2018) 'Changes in mainland Portuguese forest areas since the last decade of the XXth century', *Mediterranee* [Preprint], (130). Available at: https://doi.org/10.4000/MEDITERRANEE.10025.

Bohn, U., Hettwer, C. and Gollub, G. (2005) *Application and Analysis of the Map of the Natural Vegetation of Europe*. Bonn.

Buckley, T.N. (2019) 'How do stomata respond to water status?', *New Phytologist*. Blackwell Publishing Ltd, pp. 21–36. Available at: https://doi.org/10.1111/nph.15899.

Büttner, G. *et al.* (2017) *Final CLC2018 Technical Guidelines*.

Caltech TROPOMI SIF Data. (2021). Data from the TROPOspheric Monitoring Instrument (TROPOMI) on the Sentinel-5P satellite, providing observations of solar-induced fluorescence (SIF) in the Earth's atmosphere. Köhler, P., Frankenberg, C. Accessed January 12, 2022. [ftp://fluo.gps.caltech.edu/data/tropomi/] via NASA Earthdata.

Caswell, T.A. *et al.* (2021) 'matplotlib/matplotlib: REL: v3.4.3'. Available at: https://doi.org/10.5281/ZENODO.5194481.

Damm, A. *et al.* (2018) 'Remote sensing of plant-water relations: An overview and future perspectives', *Journal of Plant Physiology*, 227, pp. 3–19. Available at: https://doi.org/10.1016/j.jplph.2018.04.012.

Damm, A. *et al.* (2021) 'On the seasonal relation of sun-induced chlorophyll fluorescence and transpiration in a temperate mixed forest', *Agricultural and Forest Meteorology*, 304–305. Available at: https://doi.org/10.1016/j.agrformet.2021.108386.

Damm, A., Roethlin, S. and Fritsche, L. (2018) 'Towards advanced retrievals of plant transpiration using suninduced chlorophyll fluorescence: First considerations', in *International Geoscience and Remote Sensing Symposium (IGARSS)*. Institute of Electrical and Electronics Engineers Inc., pp. 5983–5986. Available at: https://doi.org/10.1109/IGARSS.2018.8518974.

ECMWF (2018) 'IFS Documentation CY45R1 - Part IV : Physical processes', in *IFS Documentation CY45R1*. ECMWF.

Elson, P. *et al.* (2020) 'SciTools/cartopy: Cartopy 0.18.0'. Available at: https://doi.org/10.5281/ZENODO.3783894.

Eurostat (2021) *Eurostat regional yearbook 2021 edition*. Luxembourg. Available at: https://doi.org/10.2785/762788.

Fisher, J.B. *et al.* (2017) 'The future of evapotranspiration: Global requirements for ecosystem functioning, carbon and climate feedbacks, agricultural management, and water resources', *Water Resources Research*. Blackwell Publishing Ltd, pp. 2618–2626. Available at: https://doi.org/10.1002/2016WR020175.

Guanter, L. *et al.* (2021) 'The TROPOSIF global sun-induced fluorescence dataset from the Sentinel-5P TROPOMI mission', *Earth System Science Data*, 13(11), pp. 5423–5440. Available at: https://doi.org/10.5194/essd-13-5423-2021.

Hassanzadeh, E. *et al.* (2014) 'Managing water in complex systems: An integrated water resources model for Saskatchewan, Canada', *Environmental Modelling and Software*, 58, pp. 12–26. Available at: https://doi.org/10.1016/j.envsoft.2014.03.015.

Heck, K. *et al.* (2020) 'Influence of Radiation on Evaporation Rates: A Numerical Analysis', *Water Resources Research*, 56(10). Available at: https://doi.org/10.1029/2020WR027332.

Hoyer, S. and Hamman, J. (2017) 'xarray: N-D labeled Arrays and Datasets in Python', *Journal of Open Research Software*, 5(1), p. 10. Available at: https://doi.org/10.5334/jors.148.

Irmak, S. *et al.* (2003) 'Solar and Net Radiation-Based Equations to Estimate Reference Evapotranspiration in Humid Climates', *Journal of Irrigation and Drainage Engineering*, 129(5), pp. 336–347. Available at: https://doi.org/10.1061/(asce)0733-9437(2003)129:5(336).

Jarvis, A.J. and Davies, W.J. (1998) *The coupled response of stomatal conductance to photosynthesis and transpiration, Source: Journal of Experimental Botany*. Available at: https://about.jstor.org/terms.

Khaliq, A., Peroni, L. and Chiaberge, M. (2018) 'Land cover and crop classification using multitemporal sentinel-2 images based on crops phenological cycle', in *EESMS 2018 - Environmental, Energy, and Structural Monitoring Systems, Proceedings*. Institute of Electrical and Electronics Engineers Inc., pp. 1–5. Available at: https://doi.org/10.1109/EESMS.2018.8405830.

Kluyver, T. *et al.* (2016) 'Jupyter Notebooks—a publishing format for reproducible computational workflows', in *Positioning and Power in Academic Publishing: Players, Agents and Agendas - Proceedings of the 20th International Conference on Electronic Publishing, ELPUB 2016*. IOS Press BV, pp. 87–90. Available at: https://doi.org/10.3233/978-1-61499-649-1-87.

Lei, H. *et al.* (2018) 'Biological factors dominate the interannual variability of evapotranspiration in an irrigated cropland in the North China Plain', *Agricultural and Forest Meteorology*, 250–251, pp. 262–276. Available at: https://doi.org/10.1016/j.agrformet.2018.01.007.

Leng, P. *et al.* (2017) 'A practical approach for deriving all-weather soil moisture content using combined satellite and meteorological data', *ISPRS Journal of Photogrammetry and Remote Sensing*, 131, pp. 40–51. Available at: https://doi.org/10.1016/j.isprsjprs.2017.07.013.

Li, Z. *et al.* (2020) 'Solar-induced chlorophyll fluorescence and its link to canopy photosynthesis in maize from continuous ground measurements', *Remote Sensing of Environment*, 236. Available at: https://doi.org/10.1016/j.rse.2019.111420.

Lillesand, T., Kiefer, R.W. and Chipman, J. (2015) *Remote Sensing and Image Interpretation*. 7th edn. Wiley.

Lu, X. *et al.* (2018) 'Potential of solar-induced chlorophyll fluorescence to estimate transpiration in a temperate forest', *Agricultural and Forest Meteorology*, 252, pp. 75–87. Available at: https://doi.org/10.1016/j.agrformet.2018.01.017.

Ma, L. *et al.* (2022) 'Analysis on the relationship between sun-induced chlorophyll fluorescence and gross primary productivity of winter wheat in northern China', *Ecological Indicators*, 139. Available at: https://doi.org/10.1016/j.ecolind.2022.108905.

Monteith, J.L. (1965) 'Evaporation and Environment', *Symposia of the Society for Experimental Biology*, 19, pp. 205–234.

Muñoz Sabater, J. (2019) *ERA5-Land hourly data from 1981 to present, Copernicus Climate Change Service (C3S) Climate Data Store (CDS)*. Available at: https://cds.climate.copernicus.eu/cdsapp#!/dataset/10.24381/cds.e2161bac?tab=overview (Accessed: 24 October 2021).

NASA (no date) *Solar Induced Fluorescence Satellite: Level 2 SIF, NASA*. Available at: https://climatesciences.jpl.nasa.gov/sif/download-data/level-2/ (Accessed: 24 January 2022).

Ngongondo, C. *et al.* (2013) 'Evaluation of the FAO Penman-montheith, priestley- Taylor and hargreaves models for estimating reference evapotranspiration in southern malawi', *Hydrology Research*, 44(4), pp. 706–722. Available at: https://doi.org/10.2166/nh.2012.224.

Niyogi, D.S. *et al.* (1997) 'Direct estimation of stomatal resistance for meteorological applications', *Geophysical Research Letters*, 24(14), pp. 1771–1774. Available at: https://doi.org/10.1029/97GL01790.

Pastorello, G. *et al.* (2020) 'The FLUXNET2015 dataset and the ONEFlux processing pipeline for eddy covariance data', *Scientific data*, 7(1), p. 225. Available at: https://doi.org/10.1038/s41597-020-0534-3.

Penman, H.L. (1948) 'Natural evaporation from open water, bare soil and grass', *Proceedings of the Royal Society of London*, Series A, pp. 120–145. Available at: https://royalsocietypublishing.org/.

Potential Evapotranspiration | Did You Know? | National Centers for Environmental Information (NCEI) (no date). Available at: https://www.ncei.noaa.gov/access/monitoring/dyk/potential-evapotranspiration (Accessed: 31 December 2022).

Priestley, C.H.B. and Taylor R J (1972) 'On the Assessment of Surface Heat Flux and Evaporation Using Large-Scale Parameters', *Monthly Weather Review*, 100(2), pp. 81–92.

Schlesinger, W.H. and Jasechko, S. (2014) 'Transpiration in the global water cycle', *Agricultural and Forest Meteorology*, 189–190, pp. 115–117. Available at: https://doi.org/10.1016/j.agrformet.2014.01.011.

Seabold, S. and Perktold, J. (2010) *Statsmodels: Econometric and Statistical Modeling with Python*, *PROC. OF THE 9th PYTHON IN SCIENCE CONF*. Available at: http://statsmodels.sourceforge.net/.

Sellers, P.J. *et al.* (1997) *Modeling the Exchanges of Energy, Water, and Carbon Between Continents and the Atmosphere*, *SCIENCE*.

Shan, N. *et al.* (2021) 'A model for estimating transpiration from remotely sensed solar-induced chlorophyll fluorescence', *Remote Sensing of Environment*, 252. Available at: https://doi.org/10.1016/j.rse.2020.112134.

Talebmorad, H. *et al.* (2020) 'Evaluation of uncertainty in evapotranspiration values by FAO56-Penman-Monteith and Hargreaves-Samani methods Solute Transport Modeling with Homotopy Analysis Methods View project Flood Induced Seepage under Levees View project', *Article in International Journal of Hydrology Science and Technology* [Preprint]. Available at: https://doi.org/10.1504/IJHST.2020.1064813.

Tanny, J. (2022) 'Evapotranspiration Measurements and Modeling', *Water (Switzerland)*. MDPI. Available at: https://doi.org/10.3390/w14162474.

Tsakiris, G. and Vangelis, H. (2005) *Establishing a Drought Index Incorporating Evapotranspiration*.

Utset, A. *et al.* (2004) 'Comparing Penman-Monteith and Priestley-Taylor approaches as reference-evapotranspiration inputs for modeling maize water-use under Mediterranean conditions', *Agricultural Water Management*, 66(3), pp. 205–219. Available at: https://doi.org/10.1016/j.agwat.2003.12.003.

Wang, N. *et al.* (2021) 'Diurnal variation of sun-induced chlorophyll fluorescence of agricultural crops observed from a point-based spectrometer on a UAV', *International Journal of Applied Earth Observation and Geoinformation*, 96. Available at: https://doi.org/10.1016/j.jag.2020.102276.

Yassen, A.N., Nam, W.H. and Hong, E.M. (2020) 'Impact of climate change on reference evapotranspiration in Egypt', *Catena*. Elsevier B.V. Available at: https://doi.org/10.1016/j.catena.2020.104711.

Zhang, K., Kimball, J.S. and Running, S.W. (2016) 'A review of remote sensing based actual evapotranspiration estimation', *Wiley Interdisciplinary Reviews: Water*. John Wiley and Sons Inc, pp. 834–853. Available at: https://doi.org/10.1002/wat2.1168.

Zhou, K. *et al.* (2022) 'Estimating evapotranspiration using remotely sensed solar-induced fluorescence measurements', *Agricultural and Forest Meteorology*, 314. Available at: https://doi.org/10.1016/j.agrformet.2021.108800.

Zotarelli, L. *et al.* (2010) *Step by Step Calculation of the Penman-Monteith Evapotranspiration (FAO-56 Method) 1*. Available at: https://www.agraria.unirc.it/documentazione/materiale_didattico/1462_2016_412_24509.pdf (Accessed: 4 May 2022).

Acknowledgements

I would like to express my sincere thanks to my supervisor Prof. Dr. Alexander Damm. The numerous, regular meetings helped me to develop a better understanding of my data and keeping me on track. I would also like to thank Bastian Bumann, who gave me valuable insights into programming with Python and helped me to develop my programming skills during the course of the thesis. Furthermore, I would like to thank Gwendolyn Dasser for giving me valuable input on writing a scientific thesis. Last but not least I would like to thank my friends and family for their advice and company throughout my study time.

Personal Declaration

I hereby declare that the submitted thesis is the result of my own, independent work. All external sources are explicitly acknowledged in the thesis.

Place, Date

Zürich, 31.12.22

Signature